IEEE Access
Multidisciplinary ⋮ Rapid Review ⋮ Open Access Journal

Received 14 September 2024, accepted 25 September 2024, date of publication 30 September 2024,
date of current version 9 October 2024.

Digital Object Identifier 10.1109/ACCESS.2024.3469784

RESEARCH ARTICLE

A Suspended Pollination Robot With a Flexible Multi-Degrees-of-Freedom Manipulator for Self-Pollinated Plants

NAOYA MASUDA[1], MOHAMED M. KHALIL[2], SEITARO TODA[1], KOTARO TAKAYAMA[1], AYATO KANADA[3], (Member, IEEE), AND TOMOAKI MASHIMO[4], (Member, IEEE)

[1]Department of Mechanical Engineering, Toyohashi University of Technology, Toyohashi 441-8580, Japan
[2]Department of Mechanical Engineering, College of Engineering and Technology, Arab Academy for Science, Technology and Maritime Transport, Smart Village Campus, Giza 12577, Egypt
[3]Faculty of Mechanical Engineering, Kyushu University, Fukuoka 819-0395, Japan
[4]Graduate School of Natural Science and Technology, Okayama University, Okayama 700-8530, Japan

Corresponding author: Mohamed M. Khalil (m.mostafa@aast.edu)

This work was supported in part by Japan Society for the Promotion of Science (JSPS) KAKENHI under Grant 22H01446.

ABSTRACT Pollination is an essential component of plant production, but today, agricultural fields suffer from a shortage of natural pollinators due to a variety of factors. To solve this serious problem, artificial pollination has been introduced. Robotic pollinators not only help farmers with a more cost-effective and stable pollination method but also help in crop production in environments that are not suited for natural pollinators, such as greenhouses. In this paper, we propose a suspended pollination robot that moves along the rail laid on the roof of greenhouses. This robot has a flexible multi-degrees-of-freedom manipulator with two actuators: a retractable linear actuator controls the end effector with a blower to approach the flower, and a tendon-driven continuum actuator changes the orientation of the end effector. After a flower is designated by a perspective camera and close-up camera, the end effector blows the wind to shake the flower. Field tests are conducted by manual control to assess the fruit set rate of tomatoes, one of the well-known self-pollinated plants. This result becomes a benchmark for robotic pollination when manual tasks will be replaced by AI in the future.

INDEX TERMS Agriculture robots, automated pollination robots, self-pollinated plants, tomato flowers pollination, multi-degrees-of-freedom manipulators, continuum actuators.

I. INTRODUCTION

Recently, global climate change and human activities have led to a decline in natural pollination for crops worldwide, threatening the future of food production [1]. Many farmers no longer rely on natural pollination techniques and instead depend on high-cost honey bee colony rental services [2], [3]. Such a solution seems promising at first glance; however, bees are dying at alarming rates globally due to pollution, pesticides, and colony collapse disorder [4], [5]. Moreover, there are limitations to using bee colonies in some countries due to ecological risks [6], [7]. Self-pollinated plants are also at risk as the amount and timing of pollen dispersal are influenced by local weather conditions, such as temperature, precipitation, and wind speed [8], [9]. To solve these problems, artificial pollination techniques have been developed as a more cost-effective and sustainable method to improve pollination success rate.

The idea of artificial pollination has started using simple manual processes that relied on labor. Farm workers select the flowers whether they are ready for pollination and then apply one of the pollination methods such as brush pollination, pollen sprayers, and a vibrating instrument [10], [11]. However, farm workers need skills and spend a lot of time on the tasks [12]. To make up for the shortcomings of artificial pollination, many researchers have proposed automatic pollination [13]. We have witnessed the emergence of various prototypes of automatic pollination from

The associate editor coordinating the review of this manuscript and approving it for publication was Yangmin Li.

FIGURE 1. A suspended pollination robot with a flexible multi-degrees-of-freedom manipulator and a blower.

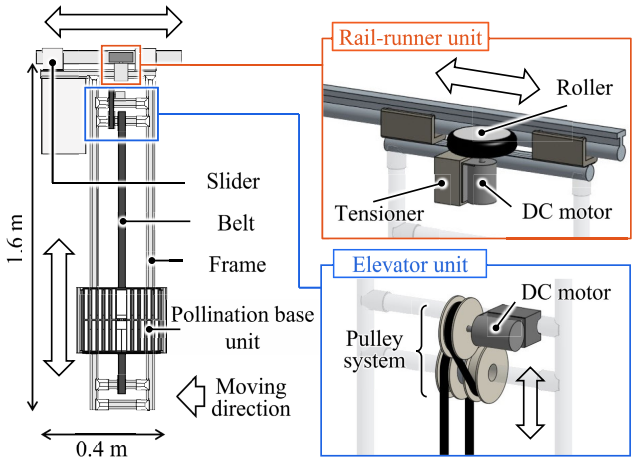

FIGURE 2. Schematic of the suspended robot: the rail-runner unit moves the robot horizontally, and the elevator unit moves the pollination base unit vertically.

ground-based to small flying robots [14]. For instance, many unmanned aerial vehicles (UAVs), also known as drones, are developed for crop pollination [15], [16], [17], [18], [19]. While most drone pollinators are fitted with an aerial broadcast pollen distributor [18], [20], other pollination modes are also investigated including the usage of the drone's air vortices to pollinate self-pollinated crops directly [21]. Furthermore, a microdrone fitted with a fur pad could emulate bees' contact pollination actions [17]; however, it is not feasible to make thousands of microdrones to replace a single honey bee colony [22]. While it has proven feasible in the outdoors, the use of UAVs in greenhouses raises several challenges, including navigation in confined spaces, indoor mapping accuracy, and wind effects on flowers.

The meticulous task of pollinating large numbers of flowers in a greenhouse is suited for ground-based robots. For example, an autonomous robot named BrambleBee was developed for pollinating bramble plants such as blackberry and raspberry using cotton brushes [23], [24]. The same robot was upgraded recently to a simultaneous multi-armed robotic pollinator to bridge the gap between pollination robots and robotic swarms [25]. Some more six-degrees-of-freedom robotic arms were also tested to pollinate watermelon and apple flowers with high position accuracy and reduced cycle time [26], [27]. Other mobile robotic platforms were used to efficiently pollinate wide areas of kiwifruits by means of a pollen sprayer [28], [29], instead of physically touching each flower. For self-pollinated crops such as tomatoes, a mobile pollination robot was designed using hormone treatment [30]. Although hormone treatment can be easily implemented since it does not require classifying flowers that can be pollinated, inappropriate hormone use may cause chemical damage and lead to quality problems such as reduced fruit shape and taste [31]. A commercially available robotic pollinator with multiple targeted air jets was also presented in the market to pollinate tomato flowers [32]. The platform also offers additional features such as diseases detection, fruit counting, and plant growth rate monitoring. Although ground pollination robots proved their functionality, they are limited to working on short plants and can only navigate on well-prepared ground.

In this paper, we present a suspended pollination robot that moves along the rail laid on the roof of greenhouses, as shown in Fig. 1. It can work regardless of the ground condition and is suited for plants at heights, e.g., tomatoes, which grow to more than 2 m (4–5 m at maximum). The flexible multi-degree-of-freedom manipulator attached to the robot controls the end effector with a blower by two actuators: a retractable linear actuator moves the end effector linearly to approach the flower, and a tendon-driven continuum actuator changes the orientation of the end effector. The pollination is performed by a blow generated by a fully pneumatic system consisting of a compressor, a tank, and a flow control valve. The flowers of the tomatoes are recognized by camera systems, and the end-effector blows the wind to shake the flowers. The field test is carried out by manual control to improve the pollination technology and to examine the standard fruit set rate for benchmarking the quality of the robot pollination.

II. MECHANICAL DESIGN

The suspended pollination robot is proposed and designed to achieve pollination according to the position and orientation of flowers. This robot controls the position of a flexible multi-degrees-of-freedom manipulator along x- and y-axes. After properly positioning the suspended robot, the manipulator approaches the flowers along z-axis, and the end effector faces the flower inflorescence.

A. SUSPENDED ROBOT

The suspended robot is designed to move along a guide rail laid at a height of approximately 1.8 meters in an experimental greenhouse. The robot mainly consists of a vertically movable unit (elevator unit), a horizontally movable unit (rail-runner unit), and a pollination base unit as shown in Fig. 2. The robot's size is slim as it measures

1.6 meters in length, 0.4 meters in width, and 0.2 meters in depth, enabling movement among plants. The frame of the robot is made of lightweight aluminum pipe structural material. The robot moves along the rails (x-axis motion) using pre-tensioned rollers that are driven by a DC-geared motor.

The pollination base unit is attached to the frame through linear bearings and moves up and down (y-axis motion) by the elevator unit. The elevator unit consists of a timing belt, a pulley system, and a DC-geared motor, as illustrated in Fig. 2. Two battery packs, which provide the necessary power to the whole robot, are placed on the back side of the timing belt and act as a counterweight for the elevator unit. In addition, a self-made marker attached to the timing belt is detected by a touch sensor, making it possible to stop at a desired height. By controlling the motion of the rail-runner and elevator units, the base unit can be moved to a desired position along x- and y-axes.

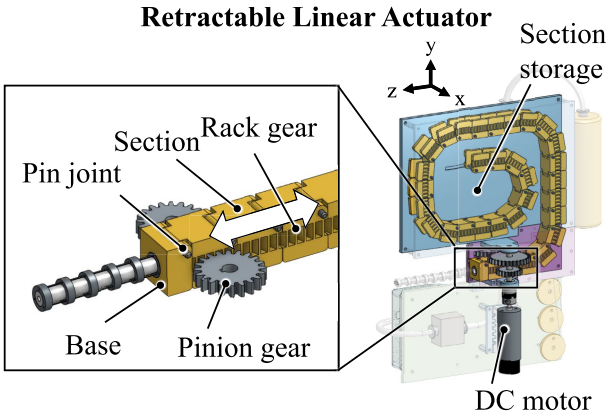

FIGURE 3. Schematic of the retractable linear actuator. The sections move linearly by the rack-and-pinion gear train, and the backward sections are retracted in the section storage.

B. MULTI-DEGREES-OF-FREEDOM MANIPULATOR

Considering the limited movable space in the greenhouse, we design a space-saving and flexible manipulator. The flexible multi-degrees-of-freedom manipulator consists of a retractable linear actuator, a small tendon-driven continuum flexible actuator, and a pneumatic system. The linear actuator allows the manipulator to approach the flowers along the z-axis, and the continuum actuator directs the tip of the end effector to all flower positions. Attached to the end effector is a soft tube that blows compressed air to shake the flowers for pollination.

1) RETRACTABLE LINEAR ACTUATOR

The pollination success rate increases by placing the end effector within the suitable distance from the flowers. Since the degrees of freedom along x- and y-axes can be achieved by the suspended robot, the degree of freedom along z-axis is required to approach the flowers. However, making the pollination robot larger in the z-axis must be avoided by design because the suspended robot moves among the plants. Thus, we designed a linear actuator with a retractable structure not to enlarge the dimension in z-axis. Fig. 3 shows the design of the retractable linear actuator. It consists of 30 independent sections linked together by metallic pin joints. The pin joints connect the sections from one end only, which allows the sections to freely rotate around the pins. A single section has a dimension of $20 \times 20 \times 19.6$ mm^3, making the total length of the linear actuator about 590 mm. To save space, the sections are stored in a section storage that has guide grooves for the metallic pins. This guide allows the actuator to be folded into a spiral shape, saving a great deal of space. The sections and the section storage are made of acrylonitrile butadiene styrene (ABS) material printed by a 3D printer.

To drive the actuator back and forth, a system of rack and pinion gears is used to transform the rotary motion of the driving motor into a linear motion of sections. The rack gears are grooved on both sides of the sections while two pinion gears (one at each side) drive the actuator. The pinion gears are linked mechanically by a system of spur gears; thus, both gears rotate simultaneously. A DC-geared motor is connected to a pinion gear through a mechanical coupling to provide the necessary driving force. A base for connecting the tendon-driven continuum actuator is placed at the end section of the actuator.

The motion of the linear actuator is measured by a rotary encoder equipped with the motor. The travel distance L of the linear actuator can be computed by the following equation:

$$L = r_{gear}\theta_{gear} \tag{1}$$

where r_{gear} and θ_{gear} are the pitch circle radius and the rotating angle of the pinion gear, respectively. The gear radius r_{gear} is set to 12.5 mm.

2) TENDON-DRIVEN CONTINUUM ACTUATOR

The orientation of flowers is random in 3D space. To increase the success rate, it is important to point the end effector directly and accurately to the anther of the flowers. The linear actuator can approach the flowers but lacks flexibility and accuracy. To overcome such drawbacks, we designed a tendon-driven continuum actuator and integrated it into the end of the linear actuator. Multiple designs of continuum manipulators have been previously reported. Some are based on sets of pre-curved concentric tubes mainly designed for minimally invasive surgeries [33], [34]. By rotating and extending the tubes with respect to each other, the position and orientation of the tip can be controlled. Other designs rely on independent pneumatically actuated chambers for manipulation [35]. Some of the latest continuum mechanisms adapt a flexible backbone structure controlled by multiple actuated tendons [36], [37]. The mechanism is directed by extending and retracting tendons with respect to each other. Inspired by that simple design, Fig. 4 shows a schematic of

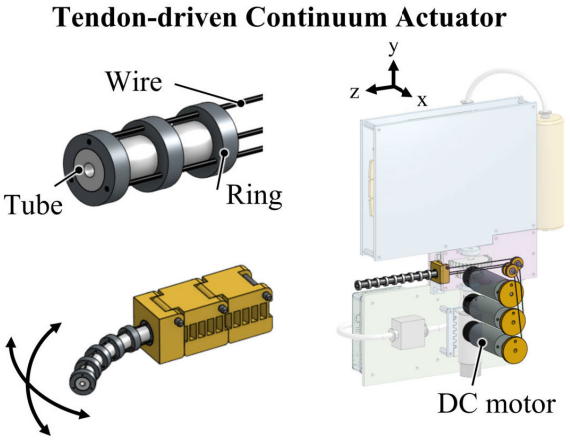

FIGURE 4. Schematic of the tendon-driven continuum actuator. The tube attached to the end of the linear actuator can bend by the three wires.

the proposed tendon-driven continuum actuator. It consists of a flexible tube, 10 hollow rings, three control wires, and a driving unit with 3 motors. The tube is made from silicon material that acts like a soft spring; it deforms when an external force is applied and returns to its original shape when the force is removed. The tube has a total length of 100 mm, an outer diameter of 6 mm, and an inner diameter of 2 mm. The hollow rings are placed with an interval of approximately 10 mm. The first ring is fixed to the tip of the silicon tube while the last one is connected to the base of the linear actuator. Three holes with a diameter of 0.5 mm are opened in every ring at a 120° interval to let the control wires get through. The wires are fixed to the first ring and connected to the driving unit at the other end. The wires are made from strong fluorocarbon material with a diameter of 0.235 mm.

The driving unit consists of 3 pulleys and 3 DC-geared motors. The bending curvature and orientation angle of the silicon tube can be controlled by adjusting the length of the control wires connected to the pulleys. Fig. 5 shows the kinematic model of the continuum mechanism. When a continuum mechanism with n number of rings is controlled to an arbitrary bend angle β and bend direction γ, assuming that the curvature of the tube is constant, the change in the length of the three wires $c_i (i = 0, 1, 2)$ can be expressed by the following equation:

$$c_i = \frac{2n}{\beta} \sin \frac{\beta}{2n} \{ n l_{tube} - r\beta \cos(\gamma + \theta_i) \} + L \qquad (2)$$

where l_{tube} is the length of the tube between the rings, r is the distance from the central axis of the arm to the wire, and θ_i indicates the position angle of the wires in the rings ($\theta_i = 0, 120, -120$).

3) PNEUMATIC SYSTEM

Self-pollinated plants, also known as hermaphroditic plants, such as tomatoes can be pollinated by natural wind. The wind shakes the flower which leads to pollen transfer from the anther (a part of the stamen) to the stigma (a part of the pistil).

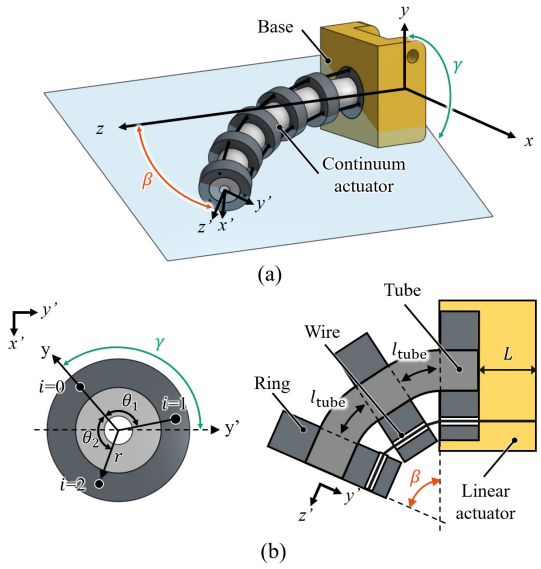

FIGURE 5. Kinematic model of the tendon-driven continuum actuator. The bending curvature and direction angle are changed by controlling the length of the wires.

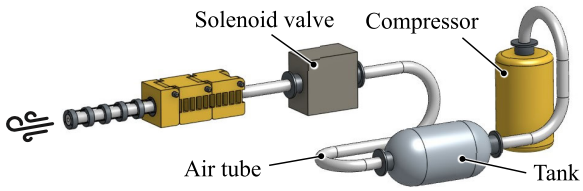

FIGURE 6. Pneumatic system to generate compressed air for producing a blow.

To create the same effect in closed spaces like greenhouses, the robot employs a system that can blow a wind. The pneumatic system consists of a compressor, a tank, and a flow control valve, as illustrated in Fig. 6. The compressor is battery-operated and can provide a maximum air pressure of 1000 kPa. The compressor shuts off automatically when the pressure reaches the pre-set value. The tank is printed by a 3D printer and has a total length of 120 mm and a diameter of 60 mm, which can store around 0.15 liter of air, enough to shake one flower. A DC pilot-operated flow control valve is placed after the tank to release the compressed air upon receiving a signal from the controller. The output of the valve is connected to the silicon tube of the continuum actuator.

III. PERFORMANCE EVALUATION OF ROBOTIC MANIPULATOR

To evaluate the proposed multi-degrees-of-freedom manipulator, all components of the manipulator are assembled as shown in Fig. 7. The pneumatic system is placed at the back side of the prototype to counterweight any forward weight bias. Several experiments are conducted to quantitatively evaluate various aspects of the approach, including wind

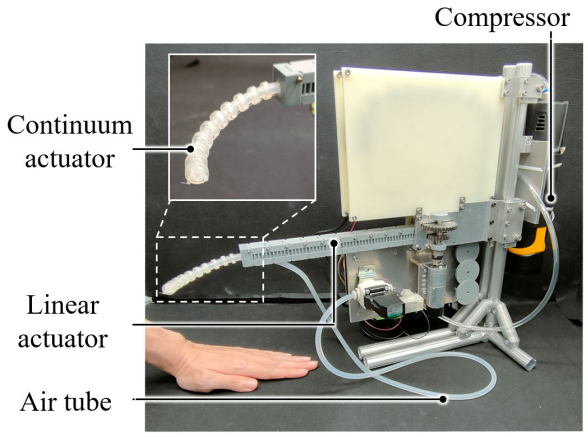

FIGURE 7. Prototype of the flexible multi-degrees-of-freedom manipulator with a pneumatic blower.

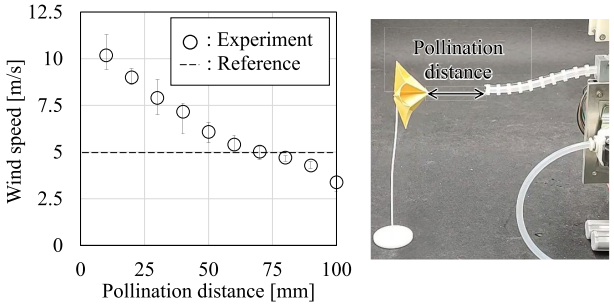

FIGURE 8. The wind speed when the pollination distance between the blower and the anemometer is changed.

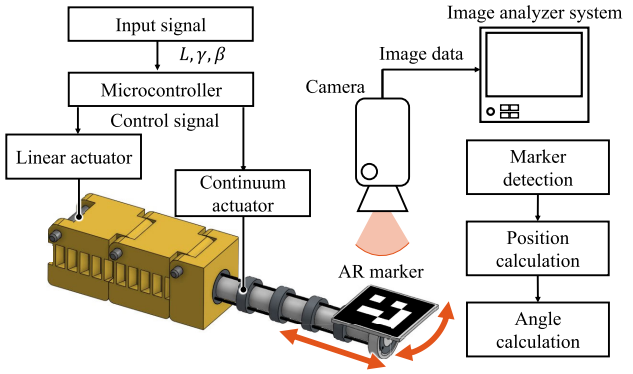

FIGURE 9. Experimental setup to evaluate the positioning accuracy of the linear actuator and the continuum actuator.

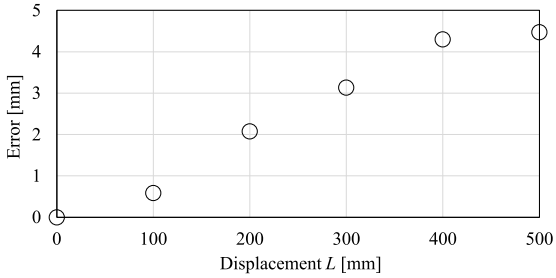

FIGURE 10. Displacement error of the retractable linear actuator when the desired displacements with an interval of 100 mm are given.

effect optimization and the positioning accuracy of the manipulator to reach flowers in different postures.

A. BLOW OPTIMIZATION

The blow needs to be optimized by the wind speed and the distance so that the success rate of pollination increases; a weak wind cannot shake the flowers properly, while a too-strong wind can rip off the flowers from the plant. Although there is little information on wind speed, a report shows that the pollination rate improves at wind speeds of 5 m/s in the case of tomato flowers [21]. We adjust the pressure of the compressor to a constant value of 137 kPa (around 20 PSI) and manipulate the pollination distance between the blower and the anemometer (GM816m, Shenzhen Jumaoyuan Science And Technology Co., China). Fig. 8 shows the wind speed when the distance between the blower and anemometer is changed. Considering the result of this experiment, the distance must be equal to 60 mm to improve the success rate.

B. POSITIONING ACCURACY ASSESSMENT

The positioning accuracy of the manipulator is evaluated by an imaging system. Fig. 9 shows the experimental setup. The desired motion signal is fed directly into a microcontroller (ESP32 DevKitC V4, Espressif Systems Pte. Ltd., China) that controls the posture of the linear and continuum actuators. An augmented reality (AR) marker is attached to the tip of the continuum actuator, and a webcam (STREAMCAM, Logicool Co Ltd., Tokyo, Japan) is fixed overhead to monitor the movement of the marker. Subsequent images from the webcam are accumulated and processed by an image analyzer system, leading to the position and the angle of the marker.

The accuracy evaluation of the retractable linear actuator is performed as it moves in the range of lengths L = [0–500] mm. The desired displacements are set at 100 mm apart. In this experiment, we set the initial posture of the manipulator at the origin while the bend angle β and the bend direction γ are kept constant at zero. Each desired displacement is evaluated five times in total and the results are averaged. Fig. 10 shows the error between the desired and actual displacements. The data shows that the average positioning error is approximately 1% and a maximum error of 4.5 mm at $L = 500$ mm. The error increases proportionally with L; this is mostly because of the backlash accumulated in the rack-and-pinion gear train.

As in the linear actuator, the accuracy of the continuum actuator is evaluated. The bending angle β is measured for [0–90]° as desired angles while the linear actuator is set to $L = 100$ mm, 300 mm, and 500 mm. During this experiment, the bend direction γ is kept constant at a value of 90°. Fig. 11 shows the relation between the angle error and the bending angles β at different lengths L. A better accuracy is obtained

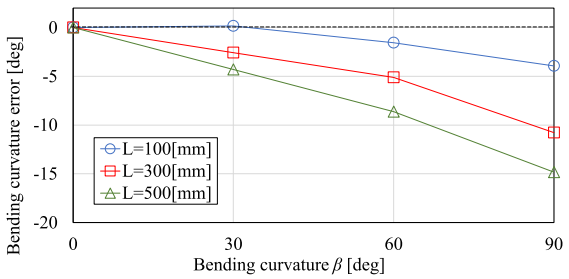

FIGURE 11. Angle error of the continuum actuator relative to a desired bending curvature β with different displacement setup.

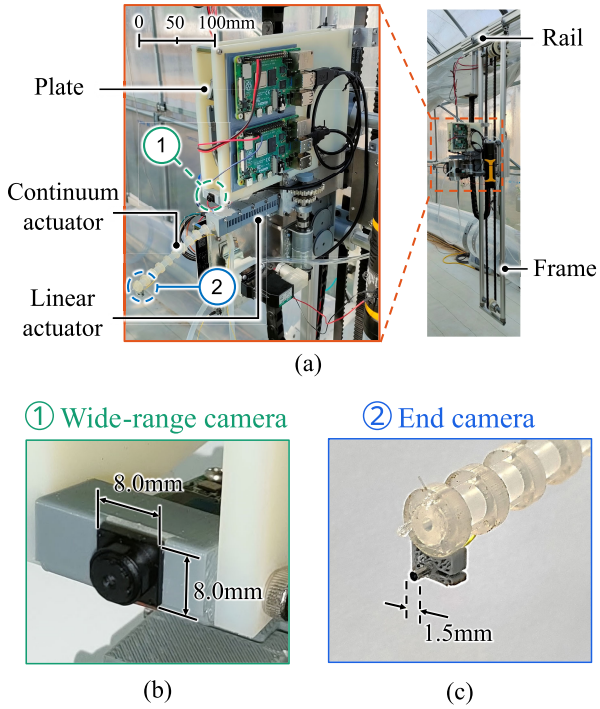

FIGURE 12. Prototype of the suspended robot with the multi-degrees-of-freedom manipulator. (a) the manipulator, (b) a wide-range camera mounted on the storage unit, and (c) a close-up camera mounted on the end effector.

when L is shorter. This is because the deformation of the mechanical wires is proportional to the wire length.

IV. PROTOTYPE OF ARTIFICIAL POLLINATION ROBOT

The prototype of the pollination robot is built by combining the manipulator with the suspended robot inside the greenhouse. As shown in Fig. 12(a), the manipulator is attached to the pollination base unit of the suspended robot so that the manipulator can move in horizontal and vertical directions. The robot can pollinate a flower located at a distance up to 520 mm along z-axis with a bending curvature β more than 180° in all bending directions. The prototype has an overall length of 1.6 m, a width of 0.4 m, and a depth of 0.3 m.

Two small cameras are mounted on the manipulator to recognize the robot and the plants. The first camera is installed at the section storage of the retractable linear

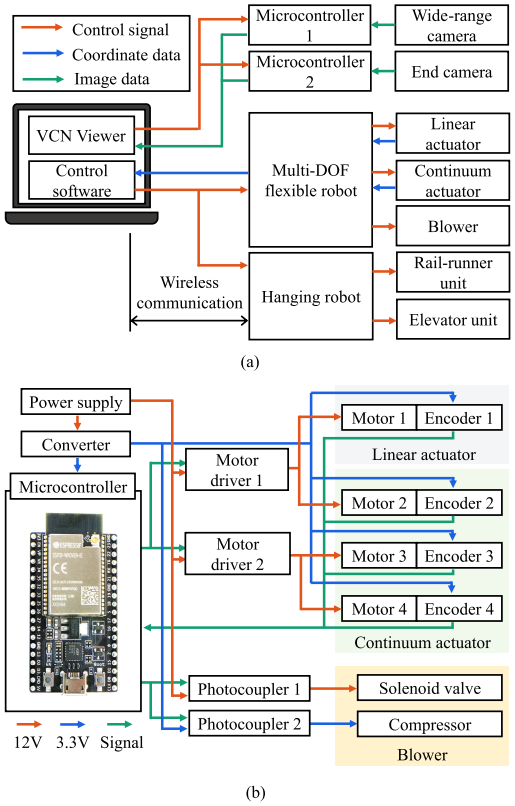

FIGURE 13. (a) Flow of the control signals for the pollination robot. (b) The flow of the power for the multi-degrees-of-freedom manipulator.

actuator as shown in Fig. 12(b). It has a resolution of 640 × 480 pixels with a frame rate of 30 fps. It is used to calibrate the position of the manipulator along x- and y-axes and to monitor the motion of the manipulator toward the flowers. The second camera is attached at the tip of the tendon-driven continuum actuator as shown in Fig. 12(c). The diameter of the camera is 1.5 mm. With a resolution of 384 × 384 pixels and 30 fps, the camera recognizes the position and the orientation of the flower.

The pollination robot employs a large-capacity battery (SGB-MDC400LP-DX, System TALKs Inc. Japan) for long-time operation. The overall weight of the robot is about 18.6 kg including the controllers and batteries. (The sufficient strength of the whole robot structure has been confirmed by stress analysis.) The robot can be fully remote-controlled from a laptop via Wi-Fi.

V. POLLINATION EXPERIMENT

A. CONTROL DIAGRAM

Fig. 13(a) shows the flow of the control signals, the coordinate data, and the image data, in the robot. The two cameras mounted on the robot are controlled by two Rasberry Pi, respectively. The recording process of the cameras starts when a remote signal is sent from the laptop to the Rasberry Pi using the software "RealVNC viewer". With a RealVNC remote connection, the captured images are displayed in

real-time. The posture of the end effector is controlled based on the images by the operator's manipulation.

The program communicates remotely with all the control loops via Wi-Fi through HTTP servers. Once a desired position is fed into the program, the control signal is sent to the motor drivers to position the robot. Similarly, all feedback signals are sent back to the program to recognize the present position.

The flow of the power to the manipulator is shown in detail in Fig. 13(b). The first microcontroller ESP32 receives the feedback signal from the encoders and supplies the power to the motors through two dual-channel motor drivers. Also, it controls the pneumatic solenoid valve and compressor by changing an on-and-off period. Meanwhile, the second ESP32 controls the posture of the suspended robot in x- and y-axes. It controls the horizontal position of the suspended robot along the rail and the vertical position of the base unit.

B. OPERATION FLOWCHART

Fig. 14 presents the flowchart of the operation of the pollination robot. The sequence starts by searching the flowers that are ready to be pollinated. In nature, flowers are found in inflorescence (referred to as a 'truss' in tomato) which can be defined as an arrangement of a cluster of flowers on the plant's branches. The location of the truss containing flowers can be confirmed visually. Once all flowers are checked widely, the robot is positioned to the front of the selected truss along x- and y-axes by driving the rail-runner and elevator units. The position of the pollination robot is set when the truss overlaps the center of the wide-range camera. After obtaining the three-dimensional coordinates of the flowers from the vision system, the new coordinates are fed to the main controller to drive the manipulator.

Once the position of the pollination robot is determined, the end effector approaches the flowers along z-axis. It is controlled by a joystick and adjusts its angle toward the flower, based on the image captured by the close-up camera. The motion of the manipulator is optimized to be collision-free; in other words, it avoids hitting the crops. After positioning the tip of the continuum actuator within 60 mm from the center of a flower, the flow control valve is triggered and the compressed air is released. Once the shaking motion of the flower is recorded, pollination is presumed to be executed and the manipulator proceeds to the next flower until the intended truss is fully pollinated. Once all flowers are treated, the manipulator is retracted and the robot heads to the next truss found by the wide-range camera.

C. EXPERIMENTAL SETUP

To demonstrate the proposed pollination robot, we select tomato flowers, a self-pollinated plant that matches the test criteria. The experiment is carried out in an experimental greenhouse set up in the courtyard of Toyohashi University of Technology, Toyohashi City, Aichi Prefecture, Japan (Fig. 15(a)). The experiments took place from December 4, 2023, to January 5, 2024. The greenhouse has an overhead

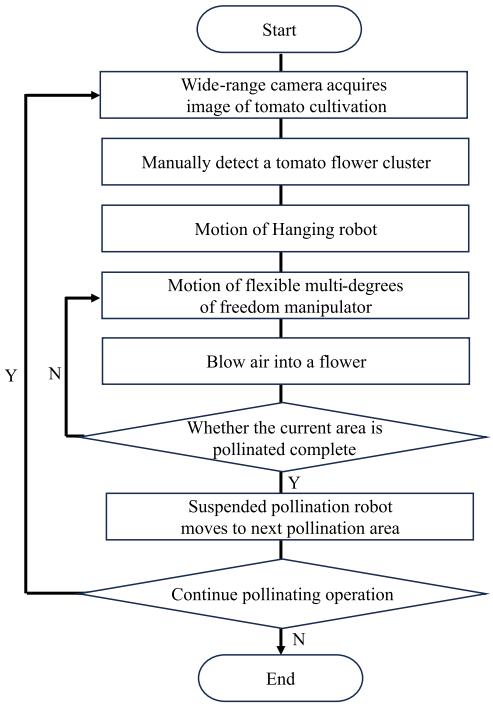

FIGURE 14. Operation flowchart of the pollination robot.

rail system installed at a height of 1.8 m from the ground. The rail system settles the robot at a distance of roughly 0.7 m away from the tomato flowers as shown in Fig. 15(b). The pollination area is located within an aluminum structure that has a height of 175 cm, a width of 180 cm, and a depth of 50 cm.

In the case of tomatoes, flowers with yellow petals are best for pollination; they are more receptive to pollen and bear fruit the same day they are pollinated. Young tomato-flower buds should be pollinated 2-3 days after fertilization to ensure fruit set. Therefore, the artificial pollination process is carried out once every three days in the morning at a temperature of 20 to 30 °C, which is known as the appropriate temperature for tomato pollination. Pollinated flowers are identified and labeled by tie papers wrapped around the flower. Plants developing fruits two weeks after pollination are considered successfully pollinated.

D. EXPERIMENTAL RESULTS

To obtain optimal pollination conditions, the distance between the flowers and the tip of the continuum actuator should be examined. The relation between the blower and the anemometer was investigated in section III. A., but measuring accurate distances to actual flowers in a greenhouse is difficult. Therefore, the experiments with two distance conditions are prepared: 0 to 50 mm and 50 to 100 mm. Furthermore, we compare these fruit set rates with the rate that is naturally pollinated outside the greenhouse. Fig. 16 shows snapshots of the flower that shakes by the blow at $t = 0$–0.2 seconds.

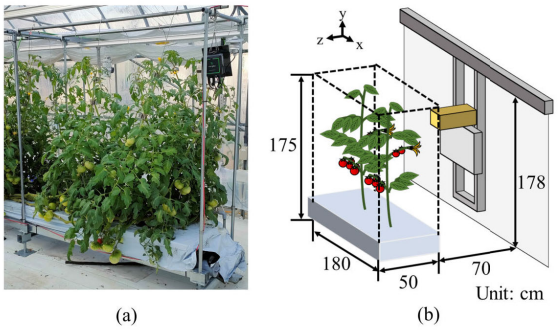

FIGURE 15. Field test for the suspended pollination robot. (a) a tomato plant in the greenhouse and (b) dimensions of the plant and the robot.

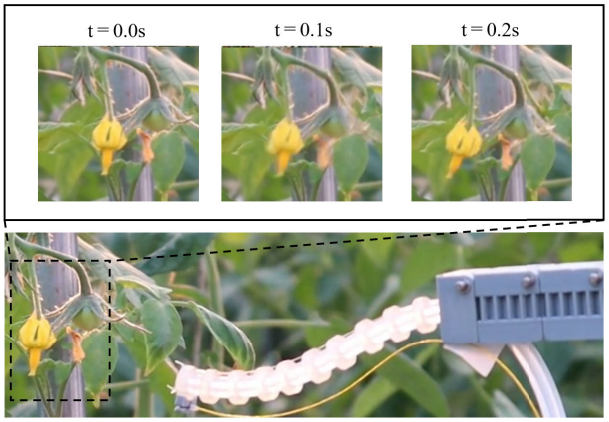

FIGURE 16. Demonstration of the robotic pollination experiment.

A total of 37 flowers were artificially pollinated by the robot in the greenhouse. In these, 23 flowers were pollinated at a distance of less than 50 mm, and the rest were pollinated at a distance of 50–100 mm. Moreover, the number of flowers ready to be naturally pollinated is visually counted. Fig. 17 presents the final experimental results. In general, flowers pollinated by the robot had a higher fruit set rate than those naturally pollinated. This result reveals a high fruit set rate of 92% for pollination at a distance of less than 50 mm. At distances larger than 50 mm, the wind speed is not sufficient due to the air viscosity, resulting in a lower fruit set rate. Since wind speeds of 5 m/s or higher are required for pollination [21], it is reasonable that good results were obtained at 50 mm or less. It is also worth mentioning that throughout all the experiments the robot was reliable and required no maintenance.

Table 1 summarizes the average time taken by each motion according to the recorded data. In total, it took less than 55 seconds for the robot to position itself in front of the target truss, extend the manipulators, and pollinate a single flower. Excluding the time required to check real-time images and input new inputs to the controller, the operating time of the robot is reduced to approximately 16.6 seconds.

Since the optimal arrangement of tomato trusses is when there are three or more flower clusters, the time required to pollinate a single flower can be significantly reduced simply by adjusting the manipulator and repeating the air blow. Under these conditions, it is expected that more than 4000 flowers can be pollinated per day by the proposed prototype, and this number will be further increased by the AI autonomous image recognition system.

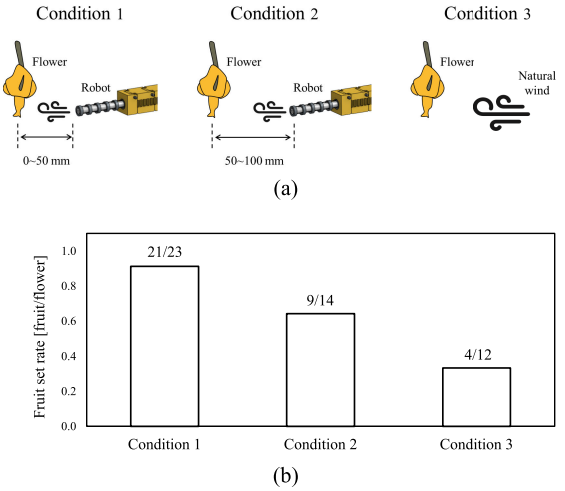

FIGURE 17. Resultant fruit set rate at different pollination conditions.

TABLE 1. Operation time of the artificial pollination robot.

Step	Working time s	Robot motion time s
Hanging robot operation	10.1	4.3
Extend pollination arm	9.9	6.0
Adjustment of arm direction	28.0	1.3
Blowing air	6.3	5.0

TABLE 2. Comparison of different pollination methods for tomatoes.

Pollination methodology	Equipment	Fruit set rate [fruit/flower]
Open pollination [38]	Bees	60%
Artificial self-pollination [38]	Tuning fork	15%
Artificial cross-pollination [38]	Tuning fork	48%
Robotic pollinator [30]	Hormone sprayer	87.5%
This work	Blasting air pulses	92%

E. PERFORMANCE EVALUATION

Table 2 compares different techniques previously reported to pollinate tomatoes in terms of fruit set rate. For open pollination, flowers are freely visited by bees under natural conditions. Artificial self-pollination flowers are sonicated daily by a tuning fork to mimic floral sonication provided by bees. The only difference for cross-pollinated flowers is that pollens from other plants are collected with the tuning fork before being dipped into the stigmas. The table also presents the data of an autonomous pollination robot for tomatoes

previously reported. Overall, robotic pollinators offer an ideal solution when compared to other techniques. Moreover, data shows that the proposed prototype demonstrates a slight improvement over the other reported robotic pollinator.

VI. CONCLUSION

In this paper, we proposed a suspended pollination robot for self-pollination plants such as tomatoes. The design criteria were presented and the optimum pollination conditions were investigated. The robot was demonstrated to pollinate tomato flowers based on camera navigation in a greenhouse environment. With the proper settings, the test result showed a 92% success rate. Since this study was a feasibility test, the robot was installed at the rail with a height of approximately 1.8 m, but it will be used with minor changes in upcoming greenhouses growing tomatoes that bear fruit 4–5 m in height.

Despite these promising results, there are still some problems that need to be solved, such as the difficulty in identifying the flower orientation and the risks associated with the remote guidance of the robot. We have already started the study to address these issues by updating the flower identification system with an AI-based image recognition system. Combining this new imaging system with high-precision mapping and localization techniques, we will make the autonomous pollination robot more effective.

REFERENCES

[1] S. G. Potts, H. T. Ngo, J. C. Biesmeijer, T. D. Breeze, L. V. Dicks, L. A. Garibaldi, R. Hill, J. Settele, and A. Vanbergen, "The assessment report of the intergovernmental science-policy platform on biodiversity and ecosystem services on pollinators, pollination and food production," Intergovernmental Sci.-Policy Platform Biodiversity Ecosystem Services (IPBES), Germany, Tech. Rep., 2016.

[2] R. E. Mallinger, H. R. Gaines-Day, and C. Gratton, "Do managed bees have negative effects on wild bees? A systematic review of the literature," *PLoS ONE*, vol. 12, no. 12, Dec. 2017, Art. no. e0189268.

[3] M. A. Aizen and L. D. Harder, "The global stock of domesticated honey bees is growing slower than agricultural demand for pollination," *Current Biol.*, vol. 19, no. 11, pp. 915–918, Jun. 2009.

[4] J. Barnett, M. Seabright, H. A. M. Williams, M. Nejati, A. J. Scarfe, J. Bell, M. H. Jones, P. Martinson, P. Schaare, and M. Duke, "Robotic pollination–targeting kiwifruit flowers for commercial application," in *Proc. PA17 Int. Tri-Conf. Precis. Agricult.*, 2017, pp. 1–9.

[5] M. A. Aizen, L. A. Garibaldi, S. A. Cunningham, and A. M. Klein, "How much does agriculture depend on pollinators? Lessons from long-term trends in crop production," *Ann. Botany*, vol. 103, no. 9, pp. 1579–1588, Jun. 2009.

[6] A. Dingley, S. Anwar, P. Kristiansen, N. W. M. Warwick, C.-H. Wang, B. M. Sindel, and C. I. Cazzonelli, "Precision pollination strategies for advancing horticultural tomato crop production," *Agronomy*, vol. 12, no. 2, p. 518, Feb. 2022.

[7] T. Nishimura, "The effect of greenhouse pollination methods on consumers' willingness to pay for tomatoes in Japan," *J. Agricult. Appl. Econ.*, vol. 53, no. 2, pp. 186–208, May 2021.

[8] C. L. Butcher, B. Y. Rubin, S. L. Anderson, and J. D. Lewis, "Pollen dispersal patterns differ among sites for a wind-pollinated species and an insect-pollinated species," *Amer. J. Botany*, vol. 107, no. 11, pp. 1504–1517, Nov. 2020.

[9] N. Yamamoto, "Human health impacts," in *Fundamentals of Bioaerosols Science*, N. Yamamoto, Ed., Amsterdam, The Netherlands: Elsevier, 2023, ch. 4, pp. 147–236.

[10] F. Aragon-Rodriguez, S. Castro-Garcia, S. Real-Moreno, H. Garcia-Mozo, R. R. Sola-Guirado, and J. Agüera-Vega, "Vibrational response of the male 'peter' pistachio branch organs to facilitate artificial pollination," *Biosyst. Eng.*, vol. 221, pp. 274–282, Sep. 2022.

[11] J. Sanghani and D. K. Varu, "Effect of different pollination methods on fruit set and yield in custard apple cv. Sindhan, annona squamosa L.," *Genetica*, vol. 22, no. 1, p. 27, 2022.

[12] T. Hiraguri, T. Kimura, K. Endo, T. Ohya, T. Takanashi, and H. Shimizu, "Shape classification technology of pollinated tomato flowers for robotic implementation," *Sci. Rep.*, vol. 13, no. 1, p. 2159, Feb. 2023.

[13] H. Castro, C. Siopa, V. Casais, M. Castro, J. Loureiro, H. Gaspar, and S. Castro, "Pollination as a key management tool in crop production: Kiwifruit orchards as a study case," *Scientia Horticulturae*, vol. 290, Dec. 2021, Art. no. 110533.

[14] M. A. Broussard, M. Coates, and P. Martinsen, "Artificial pollination technologies: A review," *Agronomy*, vol. 13, no. 5, p. 1351, May 2023.

[15] M. Mazinani, P. Zarafshan, M. Dehghani, H. Etezadi, K. Vahdati, and G. Chegini, "Modeling and control of a pollinator flying robot," in *Proc. 9th RSI Int. Conf. Robot. Mechatronics (ICRoM)*, Nov. 2021, pp. 548–553.

[16] D. Hulens, W. Van Ranst, Y. Cao, and T. Goedemé, "Autonomous visual navigation for a flower pollination drone," *Machines*, vol. 10, no. 5, p. 364, May 2022.

[17] S. A. Chechetka, Y. Yu, M. Tange, and E. Miyako, "Materially engineered artificial pollinators," *Chem*, vol. 2, no. 2, pp. 224–239, Feb. 2017.

[18] M. Mazinani, P. Zarafshan, M. Dehghani, K. Vahdati, and H. Etezadi, "Design and analysis of an aerial pollination system for walnut trees," *Biosyst. Eng.*, vol. 225, pp. 83–98, Jan. 2023.

[19] J. Shearwood, N. Aldabashi, A. Eltokhy, E. L. Franklin, N. E. Raine, C. Zhang, E. Palmer, P. Cross, and C. Palego, "C-band telemetry of insect pollinators using a miniature transmitter and a self-piloted drone," *IEEE Trans. Microw. Theory Techn.*, vol. 69, no. 1, pp. 938–946, Jan. 2021.

[20] XAG. *Saving Bees With Drones: How XAG Harnesses, 'Electronic Bees,' To Fight Against Pollination Crisis?*. Accessed: Aug. 16, 2024. [Online]. Available: https://www.xagaustralia.com.au/post/savingbeeswithdrones

[21] Q. Shi, D. Liu, H. Mao, B. Shen, X. Liu, and M. Ou, "Study on assistant pollination of facility tomato by UAV," in *Proc. ASABE Annu. Int. Meeting*, 2019, pp. 1–8.

[22] R. Gleadow, J. Hanan, and A. Dorin, "Averting robo-bees: Why free-flying robotic bees are a bad idea," *Emerg. Topics Life Sci.*, vol. 3, no. 6, pp. 723–729, Nov. 2019.

[23] N. Ohi, K. Lassak, R. Watson, J. Strader, Y. Du, C. Yang, G. Hedrick, J. Nguyen, S. Harper, D. Reynolds, C. Kilic, J. Hikes, S. Mills, C. Castle, B. Buzzo, N. Waterland, J. Gross, Y.-L. Park, X. Li, and Y. Gu, "Design of an autonomous precision pollination robot," in *Proc. IEEE/RSJ Int. Conf. Intell. Robots Syst. (IROS)*, Oct. 2018, pp. 7711–7718.

[24] J. Strader, J. Nguyen, C. Tatsch, Y. Du, K. Lassak, B. Buzzo, R. Watson, H. Cerbone, N. Ohi, C. Yang, and Y. Gu, "Flower interaction subsystem for a precision pollination robot," in *Proc. IEEE/RSJ Int. Conf. Intell. Robots Syst. (IROS)*, Nov. 2019, pp. 5534–5541.

[25] T. Smith, M. Rijal, C. Tatsch, R. M. Butts, J. Beard, R. T. Cook, A. Chu, J. Gross, and Y. Gu, "Design of stickbug: A six-armed precision pollination robot," 2024, *arXiv:2404.03489*.

[26] K. Ahmad, J.-E. Park, T. Ilyas, J.-H. Lee, J.-H. Lee, S. Kim, and H. Kim, "Accurate and robust pollinations for watermelons using intelligence guided visual servoing," *Comput. Electron. Agricult.*, vol. 219, Apr. 2024, Art. no. 108753.

[27] R. Sapkota, D. Ahmed, S. R. Khanal, U. Bhattarai, C. Mo, M. D. Whiting, and M. Karkee, "Robotic pollination of apples in commercial orchards," 2023, *arXiv:2311.10755*.

[28] K. Li, Y. Huo, Y. Liu, Y. Shi, Z. He, and Y. Cui, "Design of a lightweight robotic arm for kiwifruit pollination," *Comput. Electron. Agricult.*, vol. 198, Jul. 2022, Art. no. 107114.

[29] C. Gao, L. He, W. Fang, Z. Wu, H. Jiang, R. Li, and L. Fu, "A novel pollination robot for kiwifruit flower based on preferential flowers selection and precisely target," *Comput. Electron. Agricult.*, vol. 207, Apr. 2023, Art. no. 107762.

[30] T. Yuan, S. Zhang, X. Sheng, D. Wang, Y. Gong, and W. Li, "An autonomous pollination robot for hormone treatment of tomato flower in greenhouse," in *Proc. 3rd Int. Conf. Syst. Informat. (ICSAI)*, Nov. 2016, pp. 108–113.

[31] N. V. Obroucheva, "Hormonal regulation during plant fruit development," *Russian J. Develop. Biol.*, vol. 45, no. 1, pp. 11–21, Jan. 2014.

[32] *Website of Arugga AI Farming. Robots Treating Every Plant*. Accessed: Aug. 17, 2024. [Online]. Available: https://www.arugga.com/

[33] H. Donat, S. Lilge, J. Burgner-Kahrs, and J. J. Steil, "Estimating tip contact forces for concentric tube continuum robots based on backbone deflection," *IEEE Trans. Med. Robot. Bionics*, vol. 2, no. 4, pp. 619–630, Nov. 2020.
[34] K. A. X. J. Luo, J. Kim, T. Looi, and J. Drake, "Design optimization for the stability of concentric tube robots," *IEEE Robot. Autom. Lett.*, vol. 6, no. 4, pp. 8309–8316, Oct. 2021.
[35] P. Chaillou, J. Shi, A. Kruszewski, I. Fournier, H. A. Wurdemann, and C. Duriez, "Reduced finite element modelling and closed-loop control of pneumatic-driven soft continuum robots," in *Proc. IEEE Int. Conf. Soft Robot. (RoboSoft)*, Apr. 2023, pp. 1–8.
[36] A. L. Orekhov, E. Z. Ahronovich, and N. Simaan, "Lie group formulation and sensitivity analysis for shape sensing of variable curvature continuum robots with general string encoder routing," *IEEE Trans. Robot.*, vol. 39, no. 3, pp. 2308–2324, Mar. 2023.
[37] A. Kanada and T. Mashimo, "Switching between continuum and discrete states in a continuum robot with dislocatable joints," *IEEE Access*, vol. 9, pp. 34859–34867, 2021.
[38] S. S. Greenleaf and C. Kremen, "Wild bee species increase tomato production and respond differently to surrounding land use in northern California," *Biol. Conservation*, vol. 133, no. 1, pp. 81–87, Nov. 2006.

NAOYA MASUDA was born in 1999. He received the B.Sc. and M.Sc. degrees from Toyohashi University of Technology, Japan, in 2022 and 2024, respectively. He is currently with Mitsubishi Electric Corporation. His research interests include robots and control structure.

MOHAMED M. KHALIL received the Ph.D. degree in mechanical engineering from Toyohashi University of Technology, Japan, in 2023. He conducted some research for his master's thesis with Sapienza University of Rome, Italy, in 2017. He is currently an Assistant Professor in mechanical engineering with the Arab Academy for Science, Technology and Maritime Transport, Egypt. His research interests include micro piezoelectric actuators, control design, agriculture robots, and insect-scale robots.

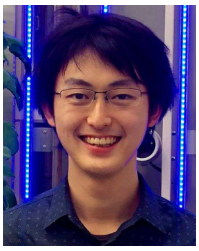

SEITARO TODA received the Ph.D. degree in agricultural science from Ehime University, Ehime, Japan, in 2020. He was an Assistant Professor with Toyohashi University of Technology, Aichi, Japan, from 2020 to 2023. His research interests include plant phenotyping and image analysis.

KOTARO TAKAYAMA received the Ph.D. degree from the Department of Biological and Environmental Engineering, Graduate School of Agricultural and Life Science, The University of Tokyo, Japan, in 2004. Throughout his academic carrier, he received 18 awards for his publications and scientific works. He is currently a Professor with the Mechanical Engineering Department, Toyohashi University of Technology, Toyohashi, Japan.

AYATO KANADA (Member, IEEE) received the Ph.D. degree in mechanical engineering from Toyohashi University of Technology, Aichi, Japan, in 2020. He is currently an Assistant Professor with the Mechanical Engineering Department, Kyushu University, Fukuoka, Japan.

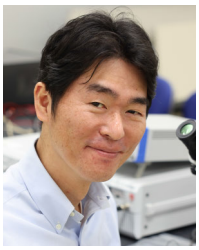

TOMOAKI MASHIMO (Member, IEEE) received the Ph.D. degree in mechanical engineering from Tokyo University of Agriculture and Technology, Fuchu, Japan, in 2008. He was a Robotics Researcher with the Robotics Institute, Carnegie Mellon University, Pittsburgh, PA, USA, from 2008 to 2010. After being an Assistant Professor (tenure-track) with the Toyohashi University of Technology, Toyohashi, Japan, in 2011, where he became an Associate Professor, in 2016. He is currently a Professor with the Graduate School of Natural Science and Technology, Okayama University, Japan. His research interests include piezoelectric actuators and robotic applications.